Surface wave surveys for imaging ground property changes due to a leaking water pipe

Ben Dashwood[1] (bendas@bgs.ac.uk)

David Gunn[1*] (dgu@bgs.ac.uk)

Giulio Curioni[2] (g.curioni@bham.ac.uk)

Cornelia Inauen[1] (cornelia@bgs.ac.uk)

Russell Swift[1] (russells@bgs.ac.uk)

David Chapman[2] (d.n.chapman@bham.ac.uk)

Alexander Royal[2] (a.c.royal@bham.ac.uk)

Peter Hobbs[1] (prnh@bgs.ac.uk)

Helen Reeves[1] (hjre@bgs.ac.uk)

Julien Taxil[3] (julien.taxil@laposte.net)

[1]British Geological Survey

Environmental Science Centre

Nicker Hill

Keyworth

Nottingham

NG12 5GG

United Kingdom

[2]Department of Civil Engineering

School of Engineering

University of Birmingham

Edgbaston

Birmingham

B15 2TT

United Kingdom

[3]Placement student at the British Geological Survey (May – July 2016);

Polytech Grenoble

14, Place du Conseil National de la Résistance

38400

St-Martin-d'Hères

France

*Corresponding author: David Gunn, [1]British Geological Survey, Environmental Science Centre, Nicker Hill, Keyworth, Nottingham, NG12 5GG, United Kingdom. Tel.: +44 (0)115 936 3400, E-mail: dgu@bgs.ac.uk

Abstract

This study demonstrates the use of Multi-channel Analysis of Surface Waves (MASW) to measure changes in Rayleigh wave velocity relating to both the initial trench construction and subsequent simulated failures (water leaks) of a buried water-pipe. The MASW field trials were undertaken in conjunction with a wider suite of geophysical monitoring techniques at a site in South-west England, within an area of clayey sandy SILT. The Rayleigh wave velocity through a soil approximately equals the shear wave velocity, which in turn is predominantly dependant on the shear modulus of the soil (G) and this can be inferred to give a measure of the relative strength of a soil. It is proposed that the time-lapse measurement of Rayleigh wave velocity may be used to monitor ongoing changes in soil strength and therefore the MASW technique could perform a significant role in monitoring the initiation/progression of any internal processes within a geotechnical asset, before they would otherwise be identified through visual inspection alone.

Keywords

Multi-channel Analysis of Surface Waves

Trench excavation

Shear modulus

Volumetric Water Content

Geophysical monitoring

1. Introduction

The continued, successful operation of buried service infrastructure relies upon the support of the natural ground / engineered soils within which they are constructed. In turn, buried services and their host materials may themselves provide support for geotechnical assets such as roads, railways or embankments for example. Within heavily urbanised areas therefore, the failure of a service could result in the ongoing degradation and loss of strength of the surrounding soil, eventually leading to a catastrophic loss of support for any overlying infrastructure. Asset maintenance and repair is often guided by visual inspection, looking for changes at the surface, or intrusive means, which themselves can compromise the overall condition of a geotechnical asset. The ability to assess soil condition around a buried service or internal to a geotechnical asset without using traditional intrusive means of investigation such as trial-pitting, would mean that alternative methods of repair, or at least, targeted ground remediation could be employed, without the need to dig-up large areas of road and before issues have manifested at the surface.

The combined network of statutory utilities beneath our city streets including water, sewer, gas and electric exceeds 1.5 million km, roughly five times the UK's road network (Parker, 2008). According to the Asphalt Industry Alliance (AIA 2013), up to 2.2 million excavations were undertaken in 2015 to repair, maintain or upgrade this network at a combined social, economic and environmental cost of £7 billion per annum (McMahon *et al.*, 2005; House of Commons, 2016). Survey methods capable of delivering anatomical ground condition information would revolutionise current remedial practice, enabling a greater range of optimised interventions as alternatives to excavation, and hence mitigate many of these disruptions. Unfortunately, modern utility survey methods such as Ground Penetrating Radar (GPR) and electromagnetic locators (e.g. CAT & Genny), specialise in utility positioning and identification (The Survey Association, 2011) and provide little quantitative information about the ground conditions and potential disturbances caused, for example by damaged utilities and associated discharges.

Common geotechnical monitoring approaches use sensors in small boreholes to directly monitor soil properties such as moisture content and pore water pressure. This is not always an efficient/effective means of relating the degree and spatial distribution of water saturation to possible water flow from a nearby leaking pipe, as such approaches include the expense of intrusive works, and only monitor a small volume of soil around the sensor, from which subsurface property changes may be quantified. Individual point sensors cannot provide continuous volumetric images of dynamic subsurface processes and a variety of different conclusions can be drawn about the cause of the ground disturbance, depending upon where the sensors are located. However, non-invasive imaging over surface-based arrays either buried just beneath the pavement or towed along the surface, offer the potential not only to provide leak early warning, but also to provide accurate location and condition monitoring of leak-affected ground.

Geophysical methods that propagate seismic waves or electric current through, and holistically sample the ground, provide alternative approaches for anatomical imaging of ground properties around the utility. Time-

lapse electrical resistivity tomography has successfully captured complex structures and groundwater movements driving deterioration, even in heterogeneous environments, with a subsurface resolution significantly closer to the true *in situ* heterogeneity than achieved using conventional intrusive or point sensing (Chambers *et al.* 2007, 2013, 2014; Gunn *et al.* 2015a). Surface wave surveys provide a reliable means of non-invasively imaging the shear wave velocity and associated stiffness distributions within engineered structures (Gunn *et al.* 2006; Gunn *et al.* 2016; Bergamo *et al.* 2016). Electrical and seismic imaging applications have been successfully adapted for use at increasing scales, e.g. from kilometric to decametric. But as yet, neither technique is routinely used at metric or sub-metric scales to assess buried utilities or the ground supporting them.

Two very important parameters controlling the shear (and hence Rayleigh) wave velocity through soil are density and small strain stiffness (or modulus of shear). Stiffness is related to the shear strength of the solid framework matrix, which is strongly influenced by mineralogy, and hence, the size, shape, friction and interactions between adjacent grains comprising the soil skeleton (Gunn *et al.* 2003, Donohue & Long 2010). Density and shear strength are controlled by the degree of consolidation of the soil fabric, often expressed using the voids ratio or porosity, and the moisture content, often expressed as the proportion of saturation (Whalley *et al.* 2012, Consentini & Foti 2014). Grain-grain contact and friction increase and porosity decreases as a soil consolidates, for example with increasing burial depth. Hence, the rigidity of the skeleton increases as the soil densifies, resulting in a positive correlation between shear strength, stiffness and density (Foti 2003, Foti 2004, Richart *et al.* 1970, Ohta & Goto 1978, Hasancebi & Ulusay 2007, Robertson 2009). It is for this reason that the soil profile exhibits an increasing shear wave velocity with depth, and because different Rayleigh wave frequencies propagate in different soil depth intervals, the phase velocity is dispersive. Shear (and Rayleigh) wave velocity is not directly dependent upon shear strength, but because of these associations, it is seen as a non-invasive, qualitative proxy for assessing shear strength changes, especially in disturbed, landslipped ground and earthworks (Gunn *et al.* 2016, Uhlemann *et al.* 2016). In coarse grained soils, such as sand and gravel, the stiffness, shear strength and shear wave velocity are dependent upon the packing density of the soil grains, and are largely insensitive to saturation. However, in fine grained soils, such as the weathered Mercia Mudstone at Blagdon, these parameters are sensitive to both changes in density caused by consolidation and the fabric consistency (plasticity or deformability) controlled by saturation, usually with increasing saturation leading to reduced shear wave velocity. Hence, non-invasive shear wave velocity monitoring is a viable option for assessing the ground stiffness and its engineering performance in relation to strength, deformability and bearing capacity of utility pipes and geotechnical infrastructure.

To this end, this paper presents the application of surface wave surveys to study the ground disturbances caused, firstly by trenching during the installation of a water pipe, and secondly by the ingress of water leaking from the pipe into the surrounding formation. Repeat surveys using the Multi-channel Analysis of Surface Waves (MASW) method were utilised: i. prior to the excavation, ii. after the water pipe installation and backfill, and then after a

controlled iii. minor leak and iv. a major leak. The MASW technique provided shear wave velocity images of the ground about the water pipe, from which, with further ground density information, the ground stiffness could also be estimated. These MASW survey observations formed a component part of a larger study of the temporal and spatial ground property changes caused by the invasion into the formation of the water leaking from the pipe. Other observations of the events at this site included using: i. a non-invasive electrical resistivity tomographic imaging method to monitor the spatio-temporal evolution of the moisture invasion into the formation about the point of the leak in the pipe, and ii. a network of sensors installed in the trench to monitor the temporal changes in moisture content, temperature and electrical conductivity at specific point locations about the water pipe. While this paper focuses on the MASW method, associated papers by Curioni *et al.* (2018) and Inauen *et al.* (2016) describe the methods and results arising from observations on the sensor network and the Electrical Resistivity Tomography (ERT) array respectively.

2. Experimental set-up

2.1 Site location and host geology

This study was undertaken within the grounds of Bristol Water's Blagdon Pumping Station, which is located behind a dam on the west end of Blagdon Lake, Somerset, UK, Fig. 1. Blagdon is situated on the north flank of an eroded anticline, where water drains to the north through Carboniferous limestones of the Mendips into Blagdon Lake, which is situated on the Sidmouth Mudstone Formation of the Mercia Mudstone Group. The Sidmouth Mudstone is characterised by red-brown mudstone and siltstone, sometimes reduced to grey-green, Fig. 1a. The experimental installation required pitting to 1.2 m deep, which revealed weathered and disturbed ground including what appeared to be red-brown, soft to stiff clayey SILT with gravel and cobble-sized, dolomitic SILTSTONE and lithorelicts of what was probably the original, unweathered MUDSTONE, Fig. 1a. The site was situated in a flat, grassed area under the canopy of several large fir trees, and the ground contained a loose network of roots ranging from 1 mm to 100 mm in diameter. The canopy and water uptake from the trees resulted in ground appearing relatively dry in the near surface, especially within the topsoil, Fig. 1a.

2.2 Water pipe installation and monitoring configurations

A pit 8 m by 1.2 m by 1.2 m deep was dug, in which an 8 m long, standard 25 mm OD MDPE water pipe was run between two stop cocks at a depth of 0.7 m, Figs. 1b, c. One end of the pipe was connected via the stop cock and a flow meter to the water mains network, which had an operating pressure between 1 and 6 bar (100 – 600 kPa), while the other could be open ended or closed, controlled by its stop cock, Fig. 1c. The leak was simulated by a small 3 mm diameter hole, facing upwards, drilled into the pipe at a point between the two stop cocks. The trench was back-filled with the soil originally excavated and re-compacted using a plate compactor and digger bucket, Figs. 1b, d. The backfill was progressed in a sequence of ~200 mm thick layers, which resulted in the ground surface of the backfilled trench being approximately level with the surrounding ground.

Fig. 2 shows the layout of the 7 parallel, 36 channel, MASW arrays (including the shot locations for the far west line) relative to the back-filled trench with the centrally located leak point. The three central arrays were located over the excavated zone, with outer array pairs to the east and west located over the host formation. The findings in this paper are supported by some observations made on the sensor network (Curioni *et al.* 2019) and over the electrical resistivity grid (Inauen *et al.* 2016) also undertaken over this trench. The sensor network was installed during the backfilling process, at the leak location around the pipe at various depths within the soil column. This network was at the centre of the MASW arrays and included: temperature sensors and Time Domain Reflectometry (TDR) probes to measure soil moisture and electrical conductivity (Curioni *et al.* 2017). The sensor sampling interval was four hours, except during leak tests when the rate of sampling was increased to once per hour. Fig. 2 also shows the footprint of an electrical resistivity array comprising a 6 m x 6 m grid of 169 steel electrodes spaced at 0.5 m. Electrical resistivity tomography images were gathered using a PRIME (PRoactive Infrastructure Monitoring and Evaluation, Gunn *et al.* 2015a) system every 4 hours during the leak tests reported in this paper and every 4-6 hours at other times between April 2016 and October 2016.

2.3 Engineering geology of the site

25 mm diameter moisture-density rings were gathered from the trench wall in the upper 1.2 m near to the leak location, Fig. 3a, with further rings also gathered from the backfill. The trench was refilled using most of the original excavated material, resulting in broadly matching formation and backfill dry densities, but with a slightly drier backfill (c.f. Volumetric Water Content (VWC) in Fig. 3a). The matrix porosity, (estimated using a grain density of 2.66 $Mg.m^{-3}$), was around 49 – 55% which, combined with a highly fissured soil mass was consistent with the dry appearance. (N.B. index tests were on intact matrix material). The undrained shear strength of the intact formation matrix was tested with a hand shear vane. A strength range of 100 – 150 kPa was consistent with a stiff soil matrix, but one that appears to be highly to completely weathered and disturbed with much destructuring and fissuring of the original mudrock. Simple Guelph permeameter tests just beneath the topsoil were either aborted due to no measurable fall in the head or indicated hydraulic conductivities up to 10^{-5} $m.s^{-1}$ normally associated with sandy soils, but which was consistent with highly fissured Mercia Mudstone reported by Hobbs *et al.* (2002).

Compaction and soil-moisture characteristic curves were also measured on remoulded material taken from the excavation, Fig. 3b, and Table 1 provides a summary of the soil geotechnical properties tested. Although the *in situ* formation appeared dry, the plasticity chart (Fig. 1a) indicates that the samples taken from the formation behaved as a high plasticity, SILT of low density and high moisture content, consistent with highly weathered/destructured Mercia Mudstone (Hobbs *et al.* (2002)). [N.B. SAND/SILT/CLAY were indicated as approximately equal grain size fractions via wet sieving and sedigraph testing. The SAND fraction is considered likely to represent the incomplete breakdown of CLAY/SILT agglomerations and a significant SAND fraction is not observed using the dried/crushed bulk material (passed through a 2mm jaw-crusher), as used for the laboratory moisture content-resistivity experiments discussed below.] The backfill was compacted to a density (dry density

= 1.25Mg.m^{-3}) that was below optimum at a relatively low moisture content (VWC=31%), and, projecting this condition onto the soil-moisture characteristic curve in Fig. 3c would indicate suctions of several thousand kPa, but which would dissipate to only 10's of kPa on saturation of this material. As both saturation (Whalley *et al.* 2012) and suction (Consentini & Foti 2014) control soil stiffness, detection of their effects on the soil shear wave velocity was a key challenge of these MASW trials.

INDEX Properties

Atterberg Limit	Moisture Content	
Plastic Limit	34%	40%
Liquid Limit	57%	67%
Plasticity Index	22%	27%
Linear Shrinkage	11%	13%
Measured	***MIN***	***MAX***

P.S.A.

Type	%
Gravel	4
Sand	36
Silt	29
Clay	31

Optimum Compaction

1.40	Mg.m^{-3}
28%	GMC
39%	VMC

in situ ranges

Dry Density	1.19 - 1.36	Mg.m^{-3}
VMC	33 - 46	%
Porosity	49 - 55	%

Eng. soil type: High plasticity, clayey SILT

Table 1: Geotechnical properties of sample materials taken from the MASW/ERT test trench at the Blagdon test site, Somerset, UK.

2.4 Multi-channel analysis of surface waves (MASW) survey method

MASW surveys use the seismic field records gathered using the same receiver array configuration adopted in shallow seismic refraction and reflection surveying (Park *et al.* 1999), Fig. 4a. Our MASW surveys employed a light hammer (0.6 kg) and plate (100x100x20 mm) source, capable of providing a broad range of frequencies from 10 Hz up to 80 Hz, Fig. 4b. Two-thirds of the total seismic wave energy generated by a vertical impact propagates as Rayleigh waves (Richart *et al.*, 1970; Gunn *et al.*, 2012). These are observed as the ground surface roll that radiates from the vertical impact and are utilised in surface wave surveys. The shear wave velocity is approximately 1.1 times the Rayleigh wave velocity and is controlled by the small strain stiffness and density of the soil (Richart *et al.* 1970; Gunn *et al.* 2016). Rayleigh waves propagate with a reverse-ellipsoid particle motion within different depth intervals in the ground shown in Fig. 4a. Higher frequencies propagate within shallower, slower intervals and lower frequencies through deeper, faster intervals. For this reason, Rayleigh waves are dispersive and the ground stiffness or shear wave velocity can be imaged using field methods that propagate multi-frequency Rayleigh waves.

Using an ABEM Terraloc Mk6 field seismometer, the field records were gathered along static linear arrays comprising 36No. 10Hz geophones spaced at 0.3 m (Fig. 4a & b). These array dimensions faithfully captured wavelengths from 0.5 m - 20 m, enabling measurement of phase velocities from 40 m.s^{-1} - 200 m.s^{-1}. Fig 4a also describes the shot sequence used for each array of 36 geophones, including a 1.2 m offset, Source 1, an end of geophone line, Source 2, with a further 5 inline sources located after every 4th geophone (1.2 m intervals). Three shots were recorded and stacked at each source location and Fig. 5a shows an example of a 36-channel

field record, from which the nearest 12 channels were selected for MASW processing. This involved application of a slowness transform to calculate the phase velocities from the time delays for the energy that propagated through the array group within a series of discrete frequency bands across the 10 – 80 Hz bandwidth (McMechan & Yedlin 1981; Park *et al.* 1999). Fig. 5b shows a phase velocity-frequency characteristic typical of a 12-geophone group, also known as a field dispersion curve, which were inverted to produce a series of shear wave velocity-depth profiles, located at the mid-point of each geophone group (distributed at 1.2 m centres), as indicated in Fig 4a. Construction of each profile involved attribution of a factored shear wave velocity (usually 1·1 times Rayleigh wave velocity) to a depth equivalent to a fraction of the Rayleigh wavelength (Foti, 2003; Joh, 1996), Fig. 5c. A depth equivalent to one third the wavelength is most commonly used because a significant proportion of the particle motion in the ground associated with Rayleigh wave propagation is approximately at this depth (Gunn *et al.*, 2006; Joh, 1996; Richart *et al.*, 1970). Vertical 2D sections were constructed along each array by contour infilling using anisotropic inverse distance weighting over a grid between each of the 7 shear wave velocity–depth profiles collected along each geophone array (Gunn *et al.*, 2016). Equivalent small strain stiffness logs and sections can also be estimated using the product of the square of the shear wave velocity and the bulk density, where for example, the bulk density can be estimated from the profile sampling using simple density rings.

3. Impact of excavation, backfill and water leaks on ground properties

3.1 Monitoring Schedule

Table 2 summarises the MASW survey schedule in relation to the trench excavation and other investigations on the sensor network, which included time-lapse ERT monitoring, Cone Penetration Resistance testing (CPT) and Terrestrial Laser Scanning (TLS) of the ground surface. Effects of both the excavation and backfilling of the trench, as well as leak water ingress on the ground's shear wave velocity have been assessed using 7 MASW arrays and five CPT profiles to a depth of 2.25 m (but initially 3.5 m into the "undisturbed" formation), spaced along line array No. 3 (see Fig. 2). The trench (Trench 2 in Fig. 2) was excavated and backfilled 20-23 Oct 2015 (along with another trench used for further tests discussed in Curioni *et al.*, 2019), which was when the formation and backfill samples were gathered for the geotechnical property tests (Fig. 3). The ground level about the trench was scanned shortly after both the excavation and backfilling using a FARO X330 laser scanner. The latter level was the baseline against which further scans could indicate subsequent ground consolidation or swelling.

The impact of the excavation and backfill were investigated via comparison between the MASW surveys and CPT profiles gathered in September 2015 and again in November 2015. A further comparison between the Nov 2015 and the pre-leak surveys undertaken in April 2016 enabled further assessment of any progressive ground velocity changes that occurred over the 2015-16 winter. Comparison of the April 2015 pre- (19 April) and post-leak surveys (22 April) enabled the impact of a minor leak of 2.095 m^3 of water into the host ground on the

ground velocity distribution to be assessed. Similarly, the impact of a major leak of 20.68 m^3 (order of magnitude greater) was assessed via comparison of the Aug 2016 pre- (8 Aug) and post-leak (11 Aug) surveys.

MASW Survey Timeline	CPT Profiles	Ground Surface LIDAR	Buried Sensor Network Data Timeline	ERT Images	Leak Times	Meter Reading Start	Meter Reading End	Approx. Flow Rate lt/min	Total Leak Volume m^3
Pre-Trench	Y	N	23-Sept-2015 ***No Sensor Data***	Y - Sting *	N/A				
Post-Trench	Y	Y	12-Nov-2015 12:00 & 16:00	Y - Sting *	N/A				
Pre-Leak	Y	Y	19-Apr-2016 18:00	Y	Leak Started @ 10:00 21-Apr-16	0.09		1.5	
Syn-Leak	N	N	21-Apr-2016 17:00 & 18:00	Y		0.65	0.72	1.5	
Post-Leak	Y	Y	22-Apr-2016 10:00	Y	Leak Turned off @ 15:45 22-Apr-16	2.08	2.185	1.5	**2.095**
Pre-Leak	Y	Y	08-Aug-2016 16:00	Y	Leak Started @ 18:25 08-Aug-16	2.76		6.4	
Syn-Leak	N	Y	09-Aug-2016 12:00	Y	13:00 09-Aug-16	8.56	9.03	5.0	
Post-Leak	Y	Y	11-Aug-2016 12:00 & 16:00	Y	14:17 11-Aug-16	22.48	22.735	4.9	
					Leak Turned-off @ 18:05 11-Aug-16		23.44	4.3	**20.68**

Table 2 MASW test timeline relative to trench excavations, leak tests and other monitoring. N.b. Pre-Trench & Post-Trench ERT profiles were acquired using an AGI SuperSting meter and surface electrode array. Additionally Post-Leak MASW surveys were undertaken 1-2 hours prior to the leak being turned off.

3.2 Impact of excavation and backfilling on shear wave velocity and stiffness

The ground property changes caused by the trenching and water ingress during these trials are captured in both 1-D velocity-depth and cone penetration resistance-depth logs (Fig. 6), as well as in 2D geophysical property change sections along the longitudinal axis of the trench (Fig. 7), which present the percentage change in velocity (and resistivity) between the time of measurement and the Pre-Trench baseline velocity model constructed from the September 2015 survey. Using a time-lapse sequence of logs/sections, an interpretation of the processes driving these property changes is presented relative to three depth intervals. These intervals include: i. the 'Trench' in the upper 1.2 m, ii. a 'Sub-Trench' interval extending from the base of the trench (1.2 m) to the top of a fully saturated interval, estimated at around 2.2 m, beneath which, the interval was denoted iii. the 'Formation > 2.2 m'. Tests on auger arisings confirmed moisture contents of 45 % Gravimetric Water Content (GWC, or approx. 54 % VWC, i.e. full saturation of all pore spaces – see Table 1) between 2.25 m and 2.75 m depths in this lower interval.

The CPT data has been smoothed using a 9 point moving average to remove the chatter of lower spatial variability encountered (when driving through siltstone cobbles for example), in order to better represent the bulk soil mass changes due to the trenching and leak testing. Apart from a greater resistance in the original formation over the upper 0.3 m, which is largely attributable to a topsoil toughened by an unbroken root mat, CPT measurements taken show good overlap from 0.4 m to 1.2 m through the Trench interval between the 'Pre-

Trench' (Sept 2015) and the 'Post-Trench' (Nov 2015) profiles, with similar densities noted between the backfilled material and original formation (Fig. 6a). The increased penetration resistance noted at ~0.5m depth (Fig 6a-ii), is likely to relate to the presence of a persistent siltstone band or "skerry" within the original formation (as shown in Fig. 1a). Greater resistance throughout the Sub-Trench, post excavation (see Fig. 6A and highlighted area >3.5 MPa cone resistance-Fig. 7b ('Formation-Nov 2015')), is attributed to consolidation over this interval in response to compaction of the lower layers of the trench fill. Note that there appears to be later relaxation, especially just below the base of the trench, for example in response to subsequent leak water ingress.

Initial CPT logs to characterise the "undisturbed" Formation indicate a laterally continuous area of low cone penetration resistance (<2.5 MPa), observed at depths in excess of 2.25 m, Fig. 6a-i (Pre-/Post-Trench) and up to 3.25 m depth elsewhere in the site. This corresponds to the apparently fully saturated Formation materials, as determined from auger arisings collected during trench excavation. Whilst further CPT profiles collected during subsequent monitoring intervals do not extend into this zone, it appears to be coincident with a persistent low velocity zone characterising the upper Formation materials defined from the MASW data between 2.25 m and 3.5m depth, Fig. 6, with velocities in excess of 150m.s^{-1} characterising materials at depths greater than 4m.

3.2.1 Impact of trench on MASW; Sept 2015 – Nov 2015

Comparison is made between the 23 Sept 2015 (Pre-Trench (Fig. 6a-velocity section)) and 12 Nov 2015 (Post-Trench (Fig. 6b-velocity change section)) measurements to assess the early effects of the trench, avoiding any later progressive effects, due for example, to the different responses of the formation and the backfill to natural moisture infiltration over the 2015-2016 winter. Between the 3-7 m stations, in the centre of the trench where the greatest compaction of the backfill materials could be achieved, velocity differences were within +/- 5-10 m.s^{-1} (Fig. 6a), which is <10% change (Fig. 7b), confirming that the backfill material was re-compacted to a density approximating that of the undisturbed formation. However, notable differences can be seen on the North side of the trench, where pre-trench velocities are reduced by over 20% in the near surface. Research in this area, e.g. by Foti & Lanellotta (2004) and Consentini & Foti (2014) generally show shear wave velocities to be reduced by ground disturbances and a lowering of density. This may be the case here, with difficulties encountered when compacting the fill at the ends of the trench around the inspection chambers for the stopcocks, but there may also be other factors contributing to the velocity reduction, for example related to dissipation of the backfill suctions into the autumn. Note, there was just over a 10% increase in the low velocity formation underlying the Southern end of the trench, corresponding with the area of increased cone penetration resistance indicated in Fig 7b.

3.2.2 Further Changes Nov 2015 – April 2016

The 2015-2016 winter was particularly wet with above average rainfall in Blagdon, but no swelling of the trench fill relative to the formation was observed via comparison of the 12 Nov 2015 and 19 Apr 2016 ground surface scans. However, a line of sensors to the side of the pipe near the leak situated at all depths (10, 35, 60, 80, 100 and 120 cm-see Fig. 8a, b) registered increasing moisture content over the Trench interval. In particular, heavy

rainfall in Jan 2016 resulted in significant infiltration and a rapid increase in saturation to over 65% in the topsoil and at the base of the trench and up to 80% at around 60 cm depth. Such moisture increases would certainly lead to dissipation of the pore suctions in the fill. There is considerable contrast in the velocity in the Trench interval between Sep 2015 (Pre-Trench) and April 2016 (Pre-Leak) velocity/penetration resistance-depth profiles (Fig. 6b) and MASW velocity change section (Fig. 7c). By April 2016, the shear wave velocity distribution throughout the backfill in the Trench Interval between the 4 m and the 9 m stations had fallen to 80 - 100 $m.s^{-1}$, a 30% change, which was attributed to softening (i.e. lowering of the stiffness) of the fill in response to rain infiltration. With a bulk density, circa 1.55 $Mg.m^{-3}$, a velocity of 80$m.s^{-1}$ equates to a fill stiffness < 10 MPa. Such fill would be highly susceptible to consolidation and deformation, and hence, completely unsuitable for supporting roads or buildings. Note also, a 10 – 20% reduction in the velocities attributed to the 'Sub-Trench 1.2-2.2 m' and 'Formation > 2.2 m' to 3 m depth intervals (Fig. 7c). Again, increased saturation, certainly over the Sub-Trench 1.2-2.2 m interval would have contributed to reduced velocities in this zone (i.e. falling to between 110 – 130 ms^{-1}-Fig. 6b).

3.3 Impact of water ingress from leaking pipe

3.3.1 Minor Leak

The minor leak began at 10.00 on 21 April 2016. The 1.5 litres per minute flow rate was maintained until the leak was stopped at 15.45 on 22 April 2016. Over this period, 2.095 m^3 of water discharged from the 3 mm hole in the pipe, situated mid-trench at 0.7 m depth into the surrounding fill and formation. The Post-Leak MASW survey was undertaken at 10.00 on 22 April 2016. A negative change in the time-lapse resistivity image indicates increases in moisture, where the magnitude of the change is also indicative of the increase in saturation (Inauen *et al.* 2016). Referring to the 'April 2016 Leak' image sequence in Fig. 7d, there appears to be a narrow funnel (possibly < 0.75 m diameter in places) constraining the drainage of water from the hole in the pipe, through the lower 'Trench' and 'Sub-Trench' intervals into the fully saturated 'Formation > 2.2 m' interval. At this depth (approx. 2.2 m), the leak waters appear to drain laterally (as well as vertically). The lateral drainage appears to develop increasingly after a delay of 8 hours. The unsaturated hydraulic conductivity of the lower Sub-Trench interval is likely to be greater than the conductivity through the saturated Formation (>2.2 m), thus leading to lateral flow just above this lower level. The diameter of the drainage plume in the Formation (>2.2 m) grows with time, growing to beyond 3 m around a day after the leak began. Development after the first day of reduced resistivity above the pipe was likely due to suctions driving moisture movement into the shallow trench-fill materials. This is consistent with the moisture sensors at 100 and 120 cm depths recording full saturation (VWC 48 – 50%) shortly after the start of the leak, whereas the sensor at 35 cm shows a more gradual moisture increase, Fig. 8c (top image).

The reduced penetration resistance extending from the leak at 0.7 m depth to the top of the Formation (Fig. 6b-ii), is consistent with reduced soil consistency (softening) due to increased moisture over this interval (however, it should be stressed that the differences may also be caused by rain as well as leak water infiltration). While

overall shear wave velocity distribution throughout the trench materials appears to be largely unaffected by the minor leak, the most significant reduction of up to 15% or around 15 $m.s^{-1}$ is mapped below the leak between 2 – 3 m depths (Sub-Trench/Formation), Fig. 7c, which occurs in-line with the apparent "funnelling" evident from the ERT measurements, Fig. 7d. A pronounced reduction in penetration resistance, particularly in the Sub-Trench materials (Fig. 6b-ii), indicates that soil consistency and stiffness in the zone affected by the drainage plume were reduced. The magnitude of the velocity reduction within the trench materials is small however and only slightly greater than the velocity measurement errors (estimated at +/- 5 $m.s^{-1}$) and although it was concentrated below the leak location, the subsequent effect of a further 2.095 m^3 of water appears to have been largely masked by the preceding heavy winter rainfall (Fig. 9).

3.3.2 Major Leak

The major leak began at 18.25 on 8 Aug 2016. Flow rate at the beginning of the test was 6.4 litres per minute, reducing to around 5.0 litres per minute after the first day, but never going lower than 4.3 litres per minute during the test. The leak was stopped at 18.05 on 11 Aug 2016 after 20.68 m^3 of water had discharged into the fill and formation. The post-leak MASW survey was undertaken at 16.00 on 11 Aug 2016. Referring to the 'August 2016 Post-Leak' Resistivity Change image in Fig. 7f, a bulb of around 2m in diameter developed beneath the point of the leak. Removal of the leak water at this flow rate was not accommodated via drainage alone (as observed in the previous minor-leak test where ERT indicated the formation of a vertical drainage funnel developing through the trench fill, before lateral dispersion of the water became apparent into/through the sub-trench materials (1.2. – 2.2m)), and would have included additional lateral and upwards infiltration into the backfill (c.f. April 2016 Leak (Fig. 6d) and August 2016 Leak (Fig. 6f)). Successive resistivity images chart the progressive dilation of this bulb (Inauen *et al.*, 2016), which appears to grow continually during the test, reaching a maximum lateral diameter of 3 – 4 m, consistent with the zone equating to a 20% reduction in measured Vs (Fig. 6e). Water broke the ground's surface 68 hours after the leak began (after ~20 m^3 of water discharged). We suspect that the bulb geometry would stabilise at some point, for example to accommodate relatively steady saturated flow from the pipe, up and out into the surrounding fill/formation to eventually flow into the saturated soils in the Formation > 2.2m interval.

Post-leak CPT measurements indicate that the penetration resistance of the trench-fill materials is homogenously low (2 MPa) to a depth of 1 m, and below this, in the 'Sub-Trench' interval (1.2 – 2.2 m), penetration resistances are in-line with the "relaxed" materials (Fig. 6c-ii). This correlates well with the shear wave velocities of 65 – 100 $m.s^{-1}$ observed from the MASW data for much of the 'Trench' zone (Fig. 6c-i). The exception to this is at the southern end of the trench, where higher velocities of up to 125 $m.s^{-1}$ are observed at the base of the 'Trench' and in the 'Sub-Trench' to the south (Fig. 7e). The increased velocities within this southern 'Sub-Trench' zone are believed to relate to increased sunlight due to the reduced canopy above the southern part of the trench, in addition to the summer increase in water-uptake from the ground by the large conifers present at the test-area.

The time-lapse ERT and post-leak MASW velocity profiles indicate that a symmetrical pattern of low shear wave velocity develops around the leak position, extending through the 'Sub-Trench (1.2 – 2.2m)' materials and into the formation below to a depth of 3.5m below the leak position itself, where shear wave velocities of 115 – 125 $m.s^{-1}$ (a reduction of 10%) are evident (Fig. 6c – Aug 2016 Post-Leak). Much of the trench-fill (<1.2m) is characterised by velocities lower than 100 $m.s^{-1}$, with the lowest velocity of 65 $m.s^{-1}$ evident around the leak position itself (Fig. 6c and Fig. 9 – Trench at Leak - August 2016). Assuming a bulk density of 1.55 $Mg.m^{-3}$ would mean that the small-strain shear modulus (stiffness) of the upper trench fill materials may be reduced from 13 MPa to <8 MPa over the course of the leak experiment (<72 hours), presenting a potential loss of support to any overlying infrastructure.

The major-leak experiment significantly elevated the VWC of much of the trench fill and underlying materials to levels above the characteristic seasonal VWC. Whilst the reduction in shear wave velocity is most pronounced in the southern half of the trench (MASW stations 4 – 8 m) where a reduction in velocity in excess of 20% is observed (Fig. 7e), there is little or no change in the velocity characterising the fill materials in the northern half of the trench other than relating to the wetting up of the trench materials post back-fill (Fig 7e), which remained around 90 $m.s^{-1}$ throughout the test (Fig. 9 - Trench-South of Leak (August 2016)). While it is possible that leak water did not penetrate this far, consistent low velocities in this zone from the minor leak test undertaken in April 2016 (after a very wet winter), may also indicate the fill in the northern half of the trench has remained at near saturation throughout both monitoring periods. Water from the leak does not appear to have much effect on the ("undisturbed") formation materials adjacent to the trench however, where little or no reduction in V_s is observed (Fig. 9 - Formation East/West of Trench - August 2016).

TDR probes buried in the vicinity of the leak indicate a VWC for the bulk of the fill material of 30-35% prior to the leak (Fig. 8c – bottom), which would equate to soil suctions of several thousand kPa based on the SWCC determined for the trench fill material (Fig. 3c). During the leak VWC's of 50 – 55% are observed, suggesting that suctions would dissipate rapidly to a few hundred kPa, before recovering slightly post-leak, where an increased VWC of 35-40% is observed (after Curioni *et al.*, 2019).

4. Relevance of this Technology to Network Monitoring

Leaks are often suspected after noticeable pressure drops between network nodes and lead to visual inspections and use of listening sticks to fine-tune the leak location. However, these may have limited use in urban settings where engineered pavements and city noise obscure the audio or visual signs of leaks. Where leaks cannot be accurately located on the water network, observation of ground disturbances they cause often provides a secondary proxy to their existence. As perception of the problem always follows detection of the disturbance, approaches relying upon surface manifestations will always detect the problem later that those making sub-surface observations. Thus, approaches based on surface observations will always encounter greater ground disturbances, which will be exacerbated where these signs have been masked, e.g. by tarmac pavements as in the urban environment.

Qualitative analysis of GPR data can be used to inform further invasive investigation, but with increased acceptance, other geophysical methods could also inform design and monitor efficacy of more sophisticated, customised interventions. Improved understanding and quantification of the relationship of shear wave velocity to engineering properties, such as stiffness and density would increase acceptability and use of surface wave surveys. This method would benefit from a better understanding of how these properties change with the consistency of key UK soils. Early focus should include the control of moisture content on both matrix and clast supported fill, for example mapping shear wave velocity onto consistency, and identifying threshold values of velocity and stiffness associated with critical shrinkage, plastic and liquid limits of fine-grained materials (of various plasticities). The contribution of suction to undrained shear strength also requires further study, especially to quantify its relationship to velocity and stiffness and their sensitivity to saturation, such as from leaks. Convincing and timely delivery of this information from the research community to the buried asset owners would stimulate the take up of surface wave surveys as part of routine monitoring and management practice. Streamed, time-lapse velocity or stiffness images could provide performance metrics as part of a smarter asset network, offering the potential for earlier detection of deterioration, improved ground disturbance mapping, more timely and better optimised intervention.

5. Conclusions

MASW surface wave surveying provides a rapid, portable and non-intrusive tool to assess the condition of the ground supporting buried infrastructure. The method yields shear wave velocity and ground stiffness information, providing a useful input to characterize static and dynamic loads. Using closely spaced geophones, 2D sections can be built up from a series of inline velocity–depth profiles spaced at intervals suitable for capturing the heterogeneity even on a sub-metric level. Similarly, pseudo 3D models can also be built up via combination of 2D sections. In this manner, MASW arrays can be scaled to capture the complex heterogeneity associated with urban settings and artificial ground.

Relatively high frequencies generated from a lightweight, impulsive source enabled investigation of the shallow subsurface in which buried utilities are located. Survey measurements are repeatable, making these methods very suitable for long term monitoring of asset condition and deterioration. Shear wave velocity or stiffness changes provide a proxy for monitoring the effect of ground disturbances associated with trenching and water ingress on the strength and supporting capacity of the ground. Ground disturbances causing low velocity (or stiffness) anomalies can be localised on MASW images with high spatial resolution. Anatomical imaging is possible, including the location of stiffness contrasts between backfill and formation, and early identification of progressive ground disturbances following water leaks. Shear wave velocity reductions of up to 10% were observed in ground disturbed by a minor leak, and reductions of up to 25% in ground disturbed by a major leak. While this case study used spiked geophones, deployment of towed streamers would enable more rapid surveys, making the MASW method a useful reconnaissance and monitoring technique. Also, the non-invasive nature of MASW enables imaging through engineered pavements. Hence, MASW methods can contribute to reducing the

level of disruption associated with street works, firstly during survey, which requires no excavation, and also improved quantification and localisation of the affected ground gained from sub-surface shear wave velocity images widens the intervention options, which in the very least can lead to smaller, more focused trenches.

Acknowledgements

The contributions of Dashwood, Gunn, Inauen, Swift, Hobbs and Reeves are published with the permission of the Executive Director of the British Geological Survey (NERC). The authors gratefully acknowledge Bristol Water PLC. for allowing access onto their pumping and treatment station at Blagdon. This study was undertaken as part of the EPSRC funded Assessing the Underworld project (EP/K021699/1).

References

Archie 1942. The electrical resistivity log as an aid in determining some reservoir characteristics: Trans. Am. Inst. Mech. Eng. 146, 54-62.

Asphalt Industry Alliance, 2013. Annual Local Authority Road Maintenance (ALARM) Survey 2013. AIA Press and Information Office, London, UK.

Berg C. 2007. An effective medium algorithm for calculating water saturations at any salinity or frequency. Geophysics 72(2), E59–67.

Bergamo, P., Dashwood, B., Uhlemann, S., Swift, R., Chambers, J., Gunn, D.A. & Donohue, S. 2016. Time-lapse monitoring of climate effects on earthworks using surface waves. Geophysics 81 (2), p1-15.

Chambers, Jonathan E.; Wilkinson, Paul B.; Weller, Alan L.; Meldrum, Philip I.; Ogilvy, Richard D.; Caunt, Simon. 2007 Mineshaft imaging using surface and crosshole 3D electrical resistivity tomography: a case history from the East Pennine Coalfield, UK. Journal of Applied Geophysics, 62 (4). 324-337. https://doi.org/10.1016/j.jappgeo.2007.03.004

Chambers, J.E.; Wilkinson, P.B.; Penn, S.; Meldrum, P.I.; Kuras, O.; Loke, M.H.; Gunn, D.A.. 2013 River terrace sand and gravel deposit reserve estimation using three-dimensional electrical resistivity tomography for bedrock surface detection. Journal of Applied Geophysics, 93. 25-32.
https://doi.org/10.1016/j.jappgeo.2013.03.002

Chambers, J.E., Gunn, D.A., Wilkinson, P.B., Meldrum, P.I., Haslam, E., Holyoake, S., Kirkham, M., Kuras, O., Merritt, A., Wragg, J. 2014. 4D electrical resistivity tomography monitoring of soil moisture dynamics in an operational railway embankment. Near Surface Geophysics 12 (1), 61-72.

Consentini, R.M. & Foti, S. 2014. Evaluation and porosity and degree of saturation from seismic and electrical data. *Geotechnique* 64(4), 278-286 http://www.icevirtuallibrary.com/doi/abs/10.1680/geot.13.P.075

Curioni, G., Chapman, D.N., Metje, N., 2017. Seasonal variations measured by TDR and GPR on an anthropogenic sandy soil and the implications for utility detection. Journal of Applied Geophysics 141, 34–46.

Curioni, G., Chapman, D. N., Royal, A. C. D., Metje, N., Dashwood, B., Gunn, D. A., Inauen, C. M., Chambers, J. E., Meldrum, P. I., Wilkinson, P. B., Swift, R. T. & Reeves, H. J. 2019. TDR potential for soil condition monitoring of geotechnical assets. Canadian Geotechnical Journal, 56 (7): 942-955 https://doi.org/10.1139/cgj-2017-0618

Donohue, S. & Long, M. 2010. Assessment of sample quality in soft clay using shear wave velocity and suction measurements. Géotechnique 60(11), 883-889. doi.org/10.1680/geot.8.T.007.3741

Foti, S. 2003. Small-strain stiffness and damping ratio of Pisa clay from surface wave tests. Géotechnique 53(5): 455–461, http://dx.doi.org/10.1680/geot.2003.53.5.455.

Foti, S. & Lancellotta, R. 2004. Soil porosity from seismic velocities. Geotechnique, 54(8), 551-554. http://www.icevirtuallibrary.com/doi/abs/10.1680/geot.2004.54.8.551

Gunn *et al.* 2003. Predicting subgrade shear modulus from existing ground models. NDT & E Int. 36(3), 135-144

Gunn, D.A., Nelder, L.M., Chambers, J.E., Raines, M.R., Reeves, H.J., Boon, D., Pearson, S., Haslam, E. Carney, J., Stirling, A.B., Ghataora, G., Burrow, M., Tinsley, R.D., Tinsley, W. & Tilden-Smith, R. 2006. Assessment of railway embankment stiffness using continuous surface waves. Proceedings of the 1st International Conference on Railway Foundations, Birmingham, UK, pp. 94–106.

Gunn DA, Nelder LM, Jackson PD, Northmore KJ, Entwisle DC, Milodowski AE, Raines MR, Boardman DI, Zoumpakis A, Rogers CDF, Karri RS, Dixon N & Jefferson I. (2006). Shear Wave Velocity Monitoring of Collapsible Loessic Brickearth Soil. Q.J.E.G.H., 39, 173-188.

Gunn DA, Williams G, Raines MG, Busby, JP, Williams, JDO & Pearson, SG. 2012. Comparison of surface wave techniques to estimate shear wave velocity in a sand and gravel sequence: Holme-Pierrepont, Nottingham, UK. Q.J.E.G.H., 45(2), 139–160, http://dx.doi.org/10.1144/1470-9236/11-009.

Gunn, D.A., Chambers, J.C., Uhlemann, S., Wilkinson, J.B., Meldrum, P.I., Dijkstra, T., Wragg, J. & Hughes, P.N. Hen-Jones, R. & Glendinning S. 2015a. Moisture monitoring in clay embankments using electrical resistivity tomography. Construction & Building Materials. (92), 82-94, 2015

Gunn, DA, Williams, GW, Kessler, HW & Thorpe, S. 2015b. Development of attributed ground models for corridor assessment of surface wave propagation. Proc. ICE Transport, **168**, 6,487-498. DOI: 10.1680/jtran.14.00036

Gunn, DA, Dashwood, BAJ, Bergamo, P & Donohue, S. (2016). Aged embankment imaging and assessment using surface waves. Forensic Engineering, V169, 149-165, Nov 2016. DOIdx.doi.org/10.1680/jfoen.16.00022

Hasancebi, N, and R Ulusay (2007). Empirical correlations between shear wave velocity and penetration resistance for ground shaking assessments, *Bull. Eng. Geology and the Environment*, 66:203–213.

Hobbs, P.R.N., Hallam, J.R., Forster, A., Entwisle, D.C., Jones, L.D., Cripps, A.C., Northmore, K.J., Self, S.J. & Meakin, J.L. 2002. Engineering geology of British rocks and soils. Mudstones of the Mercia Mudstone Group. BGS Research Report RR/01/02. 106p. http://www.bgs.ac.uk/downloads/start.cfm?id=639

House of Commons, 2016. Briefing Paper. SN739. Local road maintenance, repairs and street works in England. 22p.

Inauen, C.M., Chambers, J.E., Wilkinson, P.B., Meldrum, P.I., Swift, R., Uhlemann, S., Gunn, D.A., Dashwood, B., Taxil, J. & Curioni, G. (2016). 4D ERT monitoring of subsurface water pipe leakage during a controlled field experiment. AGU Meeting, San Francisco, 12-16 December 2016.

Joh, S.H. 1996. Advances in the Data Interpretation Technique for Spectral Analysis of Surface Waves Measurements. PhD thesis, University of Texas, Austin, TX, USA. 240p.

Jones RB (1958) In-situ measurement of the dynamic properties of soil by vibration methods. Geotechnique 8(1), 1-21.

McMahon, W., Burtwell, M.H. & Evans, M. 2005. Minimising street works disruption: the real costs of street works to the utility industry and society. Tech. Rep. 05/WM/12/8, UK Water Industry Research, London, UK, 2005.

McMechan, GA. & Yedlin, MJ. 1981. Analysis of dispersive waves by wave field transformation. Geophysics, 46, 869–874.

Ohta, Y, and N Goto (1978). Empirical shear wave velocity equations in terms of characteristic soil indexes, Earthq. Eng. Struct. Dyn., 6:167–187.

Uhlemann, S., Hagedorn, S., Dashwood, B., Maurer, H., Gunn, D., Dijkstra, T. & Chambers, J. 2016. Landslide characterization using P- and S-wave seismic refraction tomography: the importance of elastic moduli. Journal of Applied Geophysics, 134, 64-76.

Park, C. B., Miller, R. D., Xia, J., 1999. Multichannel Analysis of surface waves (MASW): Geophysics, 64, (3), pp. 800-808.

Parker, J. 2008. Briefing: The real cost of street works. Proceedings of the ICE-Transport, 161(4), 175-176. http://dx.doi.org/10.1680/tran.2008.161.4.175.

Richart FE, Wood RD and Hall JR. 1970. Vibration of Soils and Foundations. Prentice-Hall, Upper Saddle River, NJ, USA. 414p.

Robertson, PK (2009). Interpretation of cone penetration tests – a unified approach, Canadian Geotech. J., 46(11):1337–1355.

The Survey Association. 2011. The essential guide to utility surveys. Issue 4, October 2011. 60p. http://www.tsa-uk.org.uk/downloads/download/

Waxman & Smits 1968. Electrical conductivities in oil-bearing shaly sands. Soc. Petroleum Engineers Jour. 8, 107-122.

Whalley, W.R., Jenkins, M & Attenborough, K.2012. The velocity of shear waves in unsaturated soil. Soil & Tillage Res. 125, 30-37 http://oro.open.ac.uk/34343/1/STILL3046aspublished.pdf

Figures:

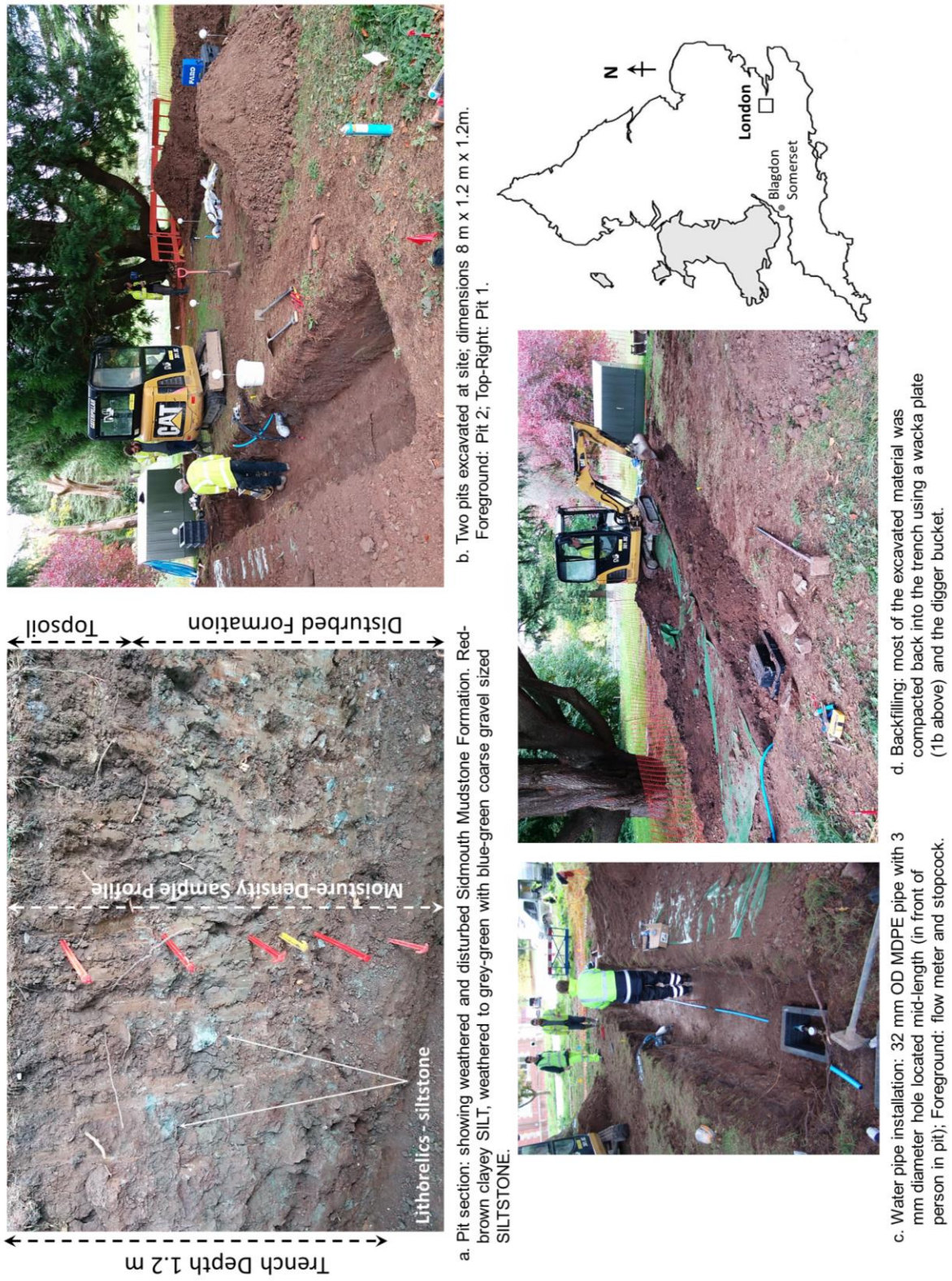

Figure 1. Site location, host geology and water pipe installation.

a. Pit section: showing weathered and disturbed Sidmouth Mudstone Formation. Red-brown clayey SILT, weathered to grey-green with blue-green coarse gravel sized SILTSTONE.

b. Two pits excavated at site; dimensions 8 m x 1.2 m x 1.2m. Foreground: Pit 2; Top-Right: Pit 1.

c. Water pipe installation: 32 mm OD MDPE pipe with 3 mm diameter hole located mid-length (in front of person in pit); Foreground: flow meter and stopcock.

d. Backfilling: most of the excavated material was compacted back into the trench using a wacka plate (1b above) and the digger bucket.

Figure 2. Monitoring instrumentation configurations for MASW, sensor network and electrical resistivity tomography. (For method and full results of sensor network monitoring see Curioni et al. 2019).

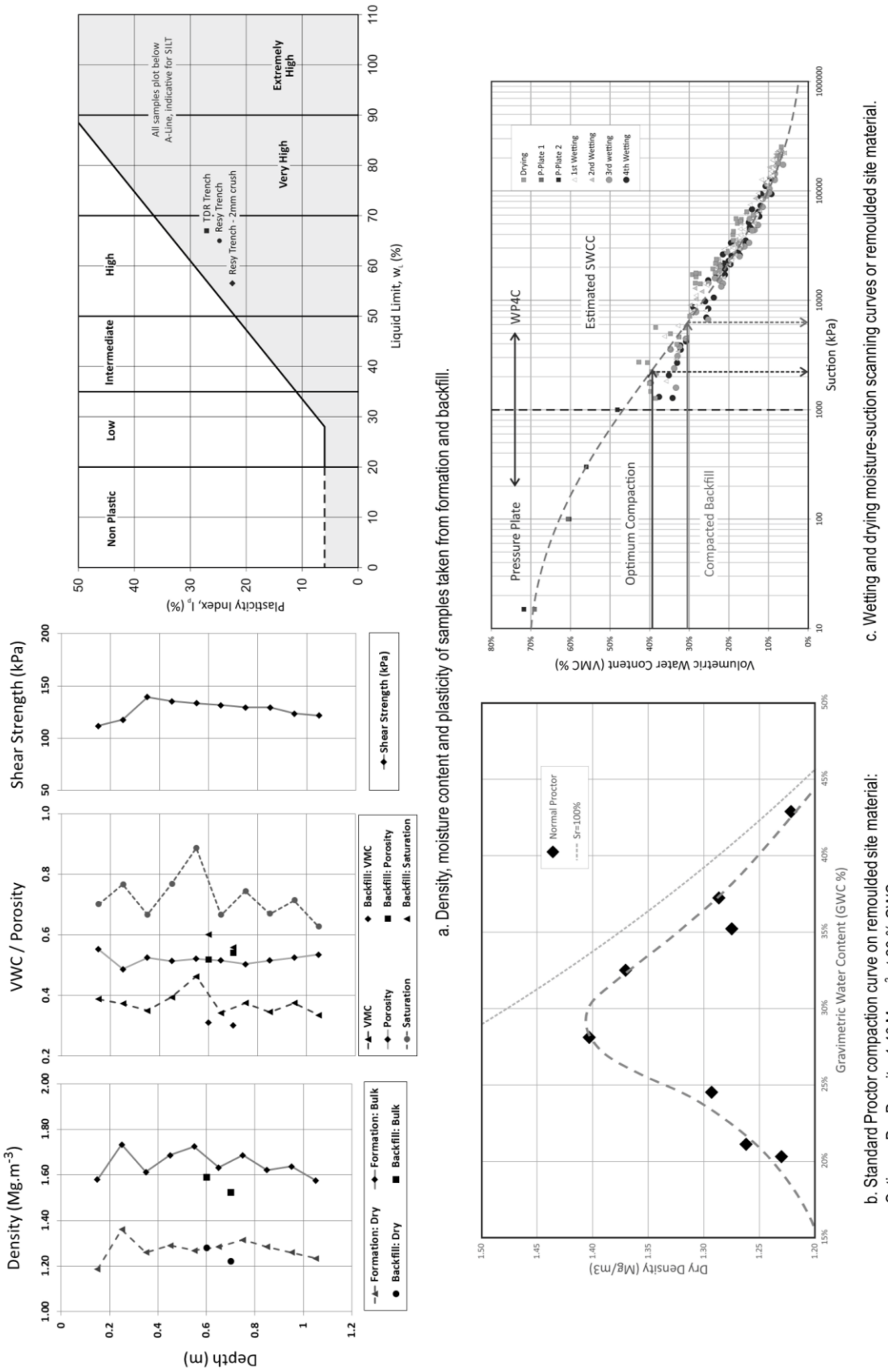

Figure 3. Geotechnical properties of in situ and remoulded samples from the formation and backfill.

a. Density, moisture content and plasticity of samples taken from formation and backfill.

b. Standard Proctor compaction curve on remoulded site material: Optimum Dry Density: 1.40 Mg.m-3 at 28 % GWC.

c. Wetting and drying moisture-suction scanning curves or remoulded site material.

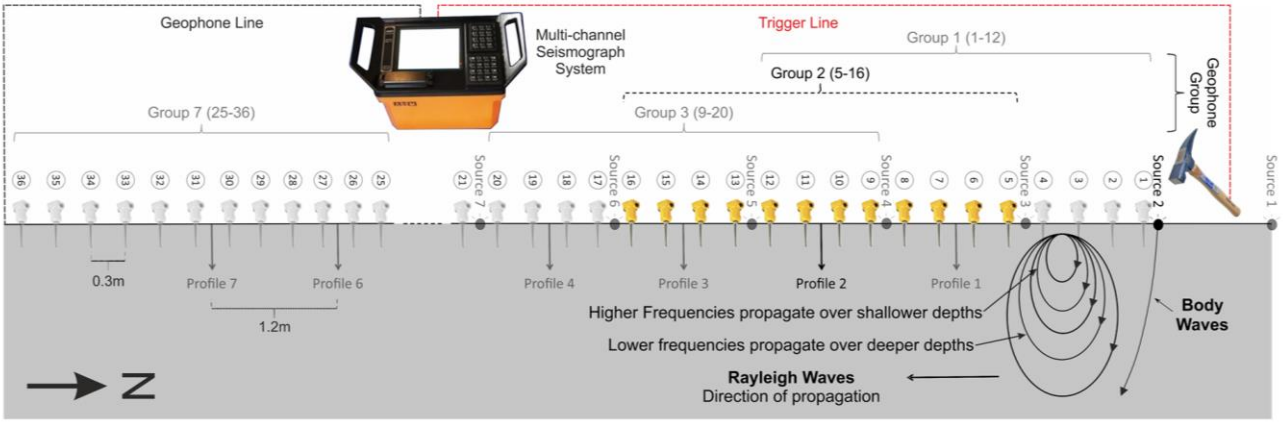

a. Schematic overview of geophone array and field seismic recorder required for MASW survey, with relative positions of 1D profiles used to generate 2D sections along each static geophone array indicated. The highlighted geophones correspond to the 12 No. "Group 2" geophones used to record the Rayleigh waves generated by "Source 2". Geophones placed at 0.3m centres, with 1.2m between shot (and therefore 1D profile) locations.

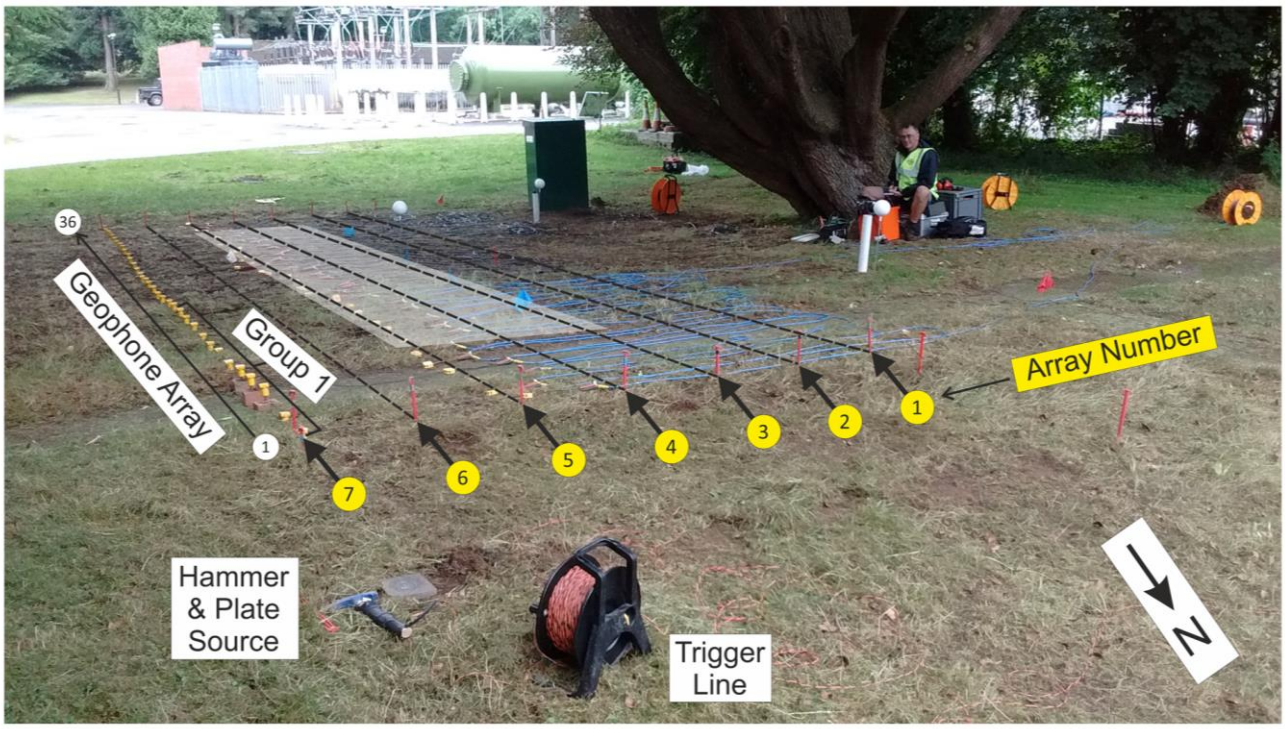

b. Photo showing the geophone arrays deployed at the field site. Reference pegs were left in place between surveys to aid re-occupation of geophone/shot locations. An array of 36 (yellow) geophones is shown deployed along Array 7 to the east of the trench (the extent of which is highlighted in grey, centred on Array 4), with the first geophone group also identified. The hammer and plate source are in the fore ground with the trigger cable running to the orange seismograph system (by the tree).

Figure 4. MASW survey using a standard field refraction seismic geophone array set-up

a. Schematic overview of geophone array and field seismic recorder required for MASW survey, with relative positions of 1D profiles used to generate 2D sections along each static geophone array indicated. The highlighted geophones correspond to the 12 No. "Group 2" geophones used to record the Rayleigh waves generated by "Source 2". Geophones placed at 0.3m centres, with 1.2m between shot (and therefore 1D profile) locations.

b. Photo showing the geophone arrays deployed at the field site. Reference pegs were left in place between surveys to aid re-occupation of geophone/shot locations. An array of 36 (yellow) geophones is shown deployed along Array 7 to the east of the trench (the extent of which is highlighted in grey, centred on Array 4), with the first geophone group also identified. The hammer and plate source are in the fore ground with the trigger cable running to the orange seismograph system (by the tree).

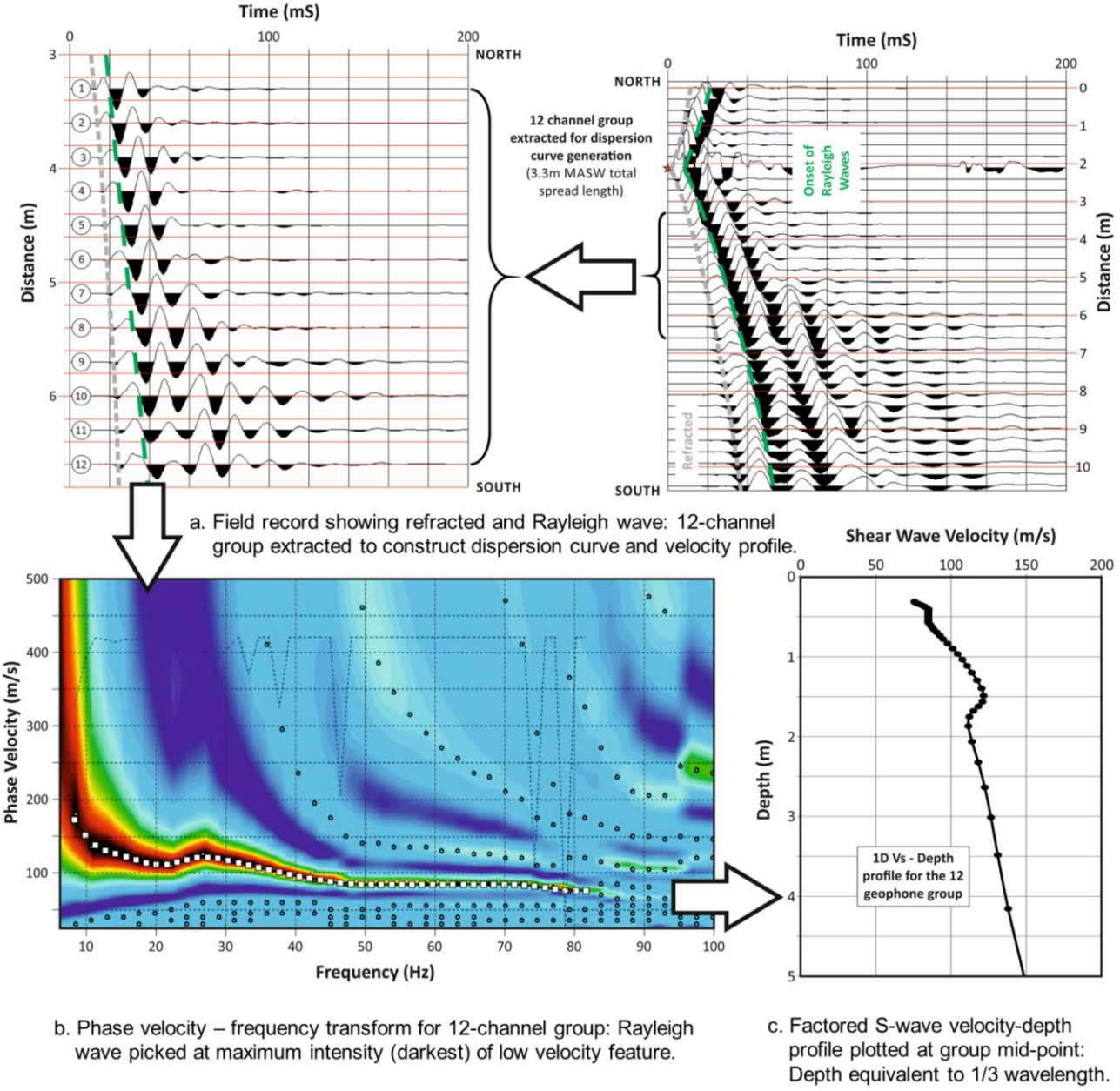

Figure 5. MASW processing steps to calculate velocity-depth logs and sections.

a. Field record showing refracted and Rayleigh wave: 12-channel group extracted to construct dispersion curve and velocity profile.

b. Phase velocity – frequency transform for 12-channel group: Rayleigh wave picked at maximum intensity (darkest) of low velocity feature.

c. Factored S-wave velocity-depth profile plotted at group mid-point: Depth equivalent to 1/3 wavelength.

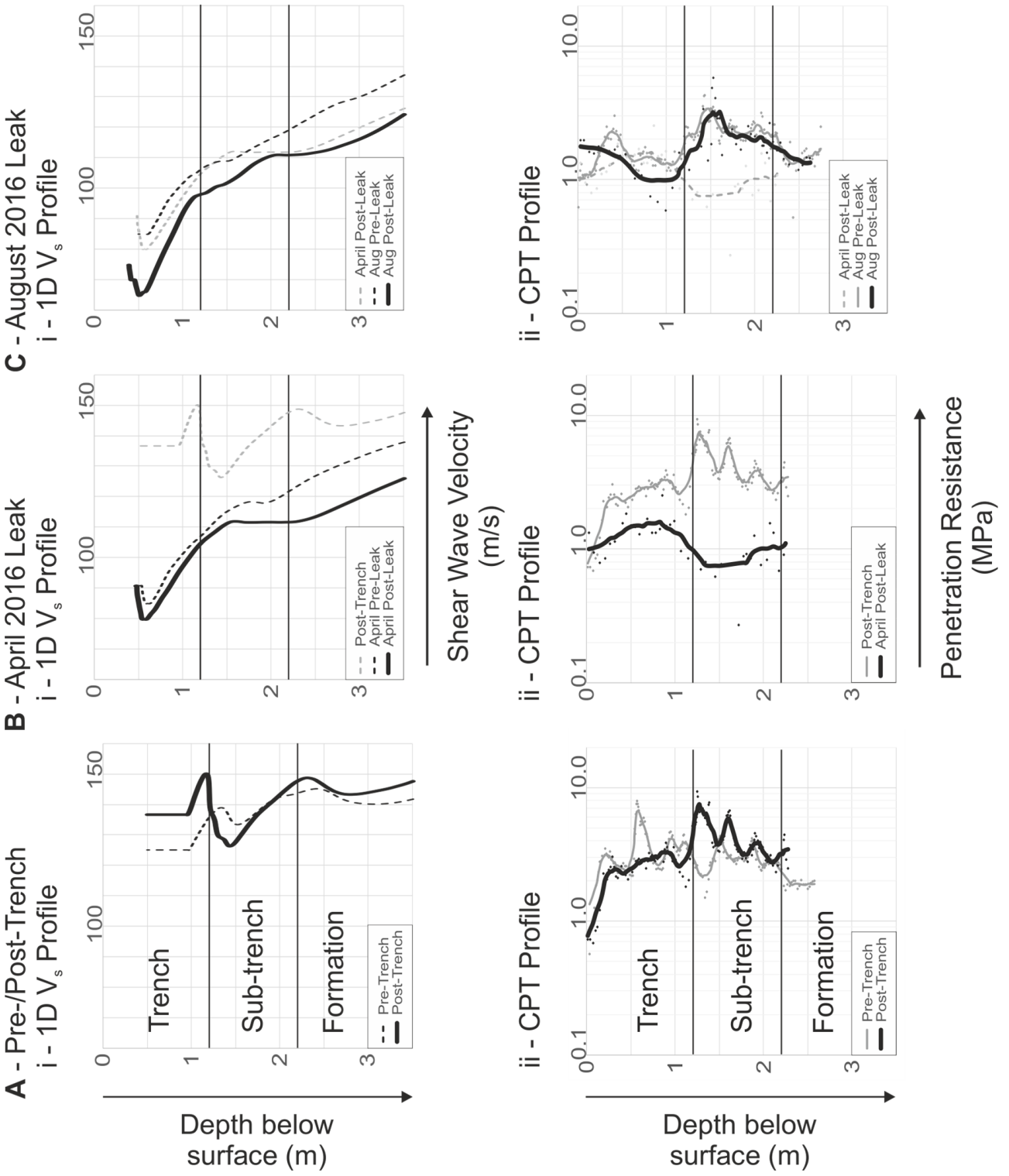

Figure 6. 1D Vs- (top) and Penetration Resistance (bottom)-Depth profiles associated with;

A-Pre-Post Trenching,

B-Pre-Post April (2016) Leak Test and

C-Pre-Post August (2016) Leak Test.

All 1D profiles refer to a position within the trench immediately adjacent to the leak location (Line 04 (Shot 04)). Vs-Depth profiles constructed as shown in Figure 5.

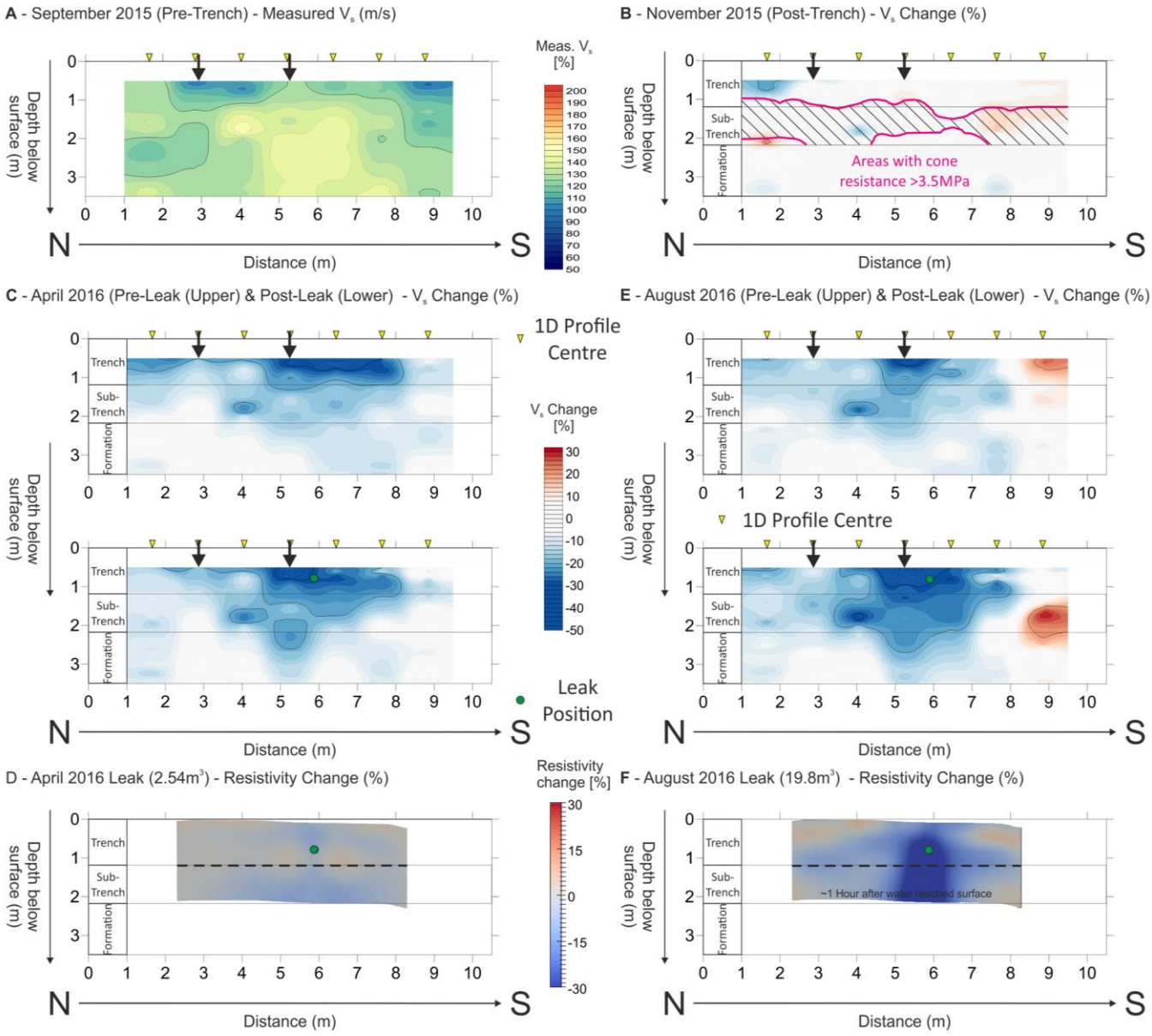

Figure 7. Changes in shear wave velocity (Vs) and resistivity in response to excavation and backfill and ingress of leak water from pipe. Velocity section for September 2015 (Pre-Trench) is used as a reference to assess change in velocity for the subsequent measurements. The same reference period is also used for the ERT data presented (see Inauen et al., 2016 for details)

a. September 2015 (Pre-Trench) – Measured Vs (m.s-1).
b. November 2015 (Post-Trench) – Vs Change (%)
c. April 2016 (Pre-Leak (Upper)) & Post-Leak (Lower) - Vs Change (%)
d. April 2016 Leak (2.54m3) – Resistivity Change (%)
e. August 2016 (Pre-Leak (Upper)) & Post-Leak (Lower) - Vs Change (%)
f. August 2016 Leak (19.8m3) – Resistivity Change (%)

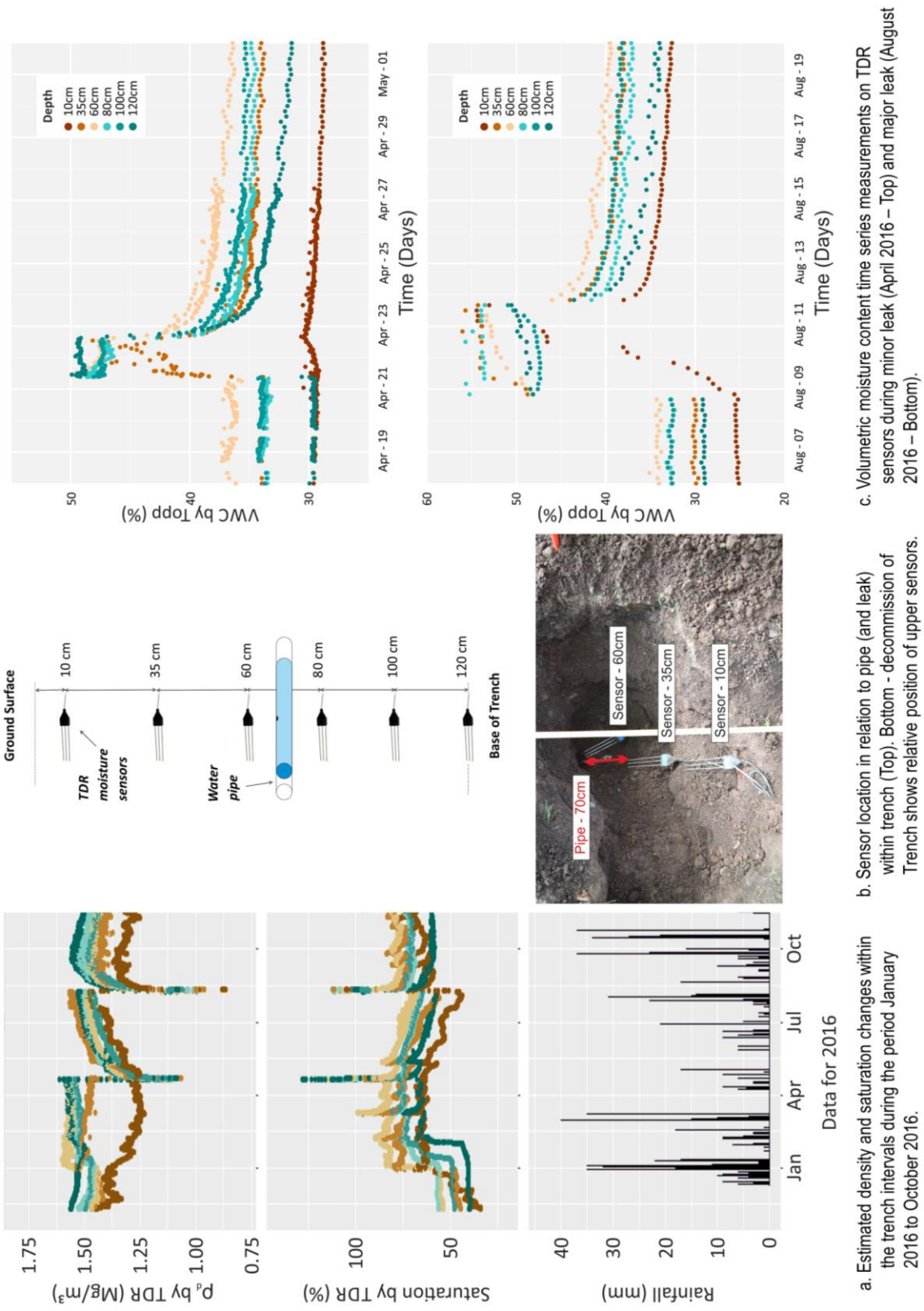

a. Estimated density and saturation changes within the trench intervals during the period January 2016 to October 2016.

b. Sensor location in relation to pipe (and leak) within trench (Top). Bottom - decommission of Trench shows relative position of upper sensors.

c. Volumetric moisture content time series measurements on TDR sensors during minor leak (April 2016 – Top) and major leak (August 2016 – Bottom).

Figure 8. Time series measurements on TDR sensors prior to and during minor leak. After Curioni et al. (2019)

a. Estimated density and saturation changes within the trench intervals during the period January 2016 to October 2016.

b. Sensor location in relation to pipe (and leak) within trench (Top). Bottom - decommission of Trench shows relative position of upper sensors.

c. Volumetric moisture content time series measurements on TDR sensors during minor leak (April 2016 – Top) and major leak (August 2016 – Bottom).

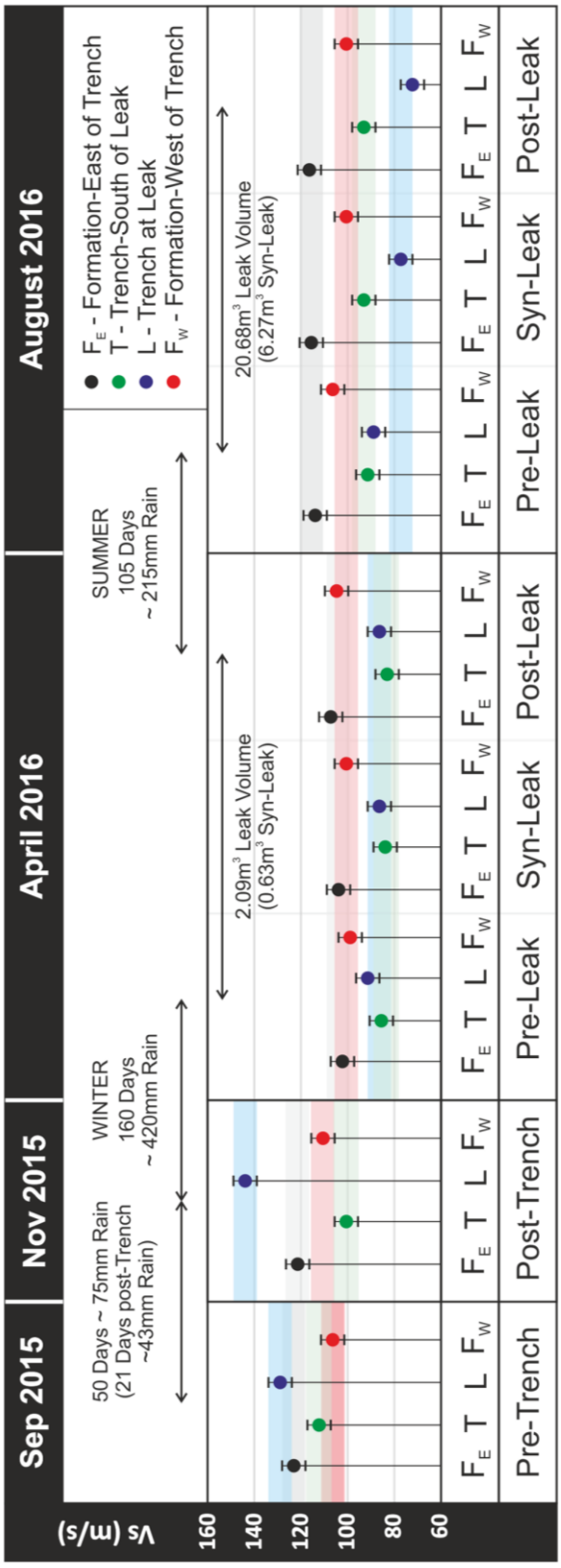

Figure 9. Comparison of average Vs derived from MASW analysis of the upper 1.2m (equivalent to the thickness trench back-fill materials).

Error bars equate to a maximum error of +/- 5m.s-1 in determining Vs. For the leak tests, coloured bars equate to the observed velocity (+/- error) of the "syn-leak" measurement for comparison with pre- and post-leak velocities.